J Mol Model (2013) 19:2689–2697
DOI 10.1007/s00894-012-1475-3

ORIGINAL PAPER

Fine structure in the transition region: reaction force analyses of water-assisted proton transfers

Diana Yepes · Jane S. Murray · Juan C. Santos · Alejandro Toro-Labbé · Peter Politzer · Pablo Jaque

Received: 28 February 2012 / Accepted: 17 May 2012 / Published online: 26 June 2012

Abstract We have analyzed the variation of the reaction force $F(\xi)$ and the reaction force constant $\kappa(\xi)$ along the intrinsic reaction coordinates ξ of the water-assisted proton transfer reactions of HX-N = Y (X,Y = O,S). The profile of the force constant of the vibration associated with the reactive mode, $k_\xi(\xi)$, was also determined. We compare our results to the corresponding intramolecular proton transfers in the absence of a water molecule. The presence of water promotes the proton transfers, decreasing the energy barriers by about 12 – 15 kcal mol^{-1}. This is due in part to much smaller bond angle changes being needed than when water is absent. The $\kappa(\xi)$ profiles along the intrinsic reaction coordinates for the water-assisted processes show striking and intriguing differences in the transition regions. For the HS-N = S and HO-N = S systems, two $\kappa(\xi)$ minima are obtained, whereas for HO-N = O only one minimum is found. The $k_\xi(\xi)$ show similar behavior in the transition regions. We propose that this fine structure reflects the degree of synchronicity of the two proton migrations in each case.

D. Yepes · J. C. Santos · P. Jaque (✉)
Facultad de Ciencias Exactas, Departamento de Ciencias Químicas, Laboratorio de Química Teórica,
Universidad Andres Bello,
Av. República 275,
Santiago, Chile
e-mail: pjaque@unab.cl

J. S. Murray (✉) · P. Politzer
CleveTheoComp LLC,
1951 W. 26th Street, Suite 409,
Cleveland, OH 44113, USA
e-mail: jsmurray@uno.edu

A. Toro-Labbé
Laboratorio de Química Teórica Computacional (QTC),
Facultad de Química, Pontifica Universidad Católica de Chile,
Casilla 306, Correo 22,
Santiago, Chile

Keywords Reaction force · Reaction force constant · Synchronicity · Transition region · Water-assisted proton transfer

Introduction

The reaction force

The reaction force $F(\xi)$ is a rigorously-based property that helps to eludicate what occurs when reactants (**R**) are converted to products (**P**), passing through a transition state (**TS**) [1–3]. From classical physics, the reaction force is the negative gradient of the potential energy $V(\xi)$ along an appropriate reaction coordinate, typically the intrinsic reaction coordinate (IRC), ξ:

$$F(\xi) = -\frac{\partial V(\xi)}{\partial \xi}. \quad (1)$$

The IRC is the path of lowest energy (steepest-descent), expressed in mass-weighted Cartesian coordinates, that leads from the transition state to the reactants and products [4, 5]. $F(\xi)$ and ξ are vectors; the latter is directed from reactants to products. Thus a positive $F(\xi)$ is driving the process toward the products, a negative $F(\xi)$ is retarding it.

For the $V(\xi)$ profiles displayed in Figs. 1a, 2a and 3a, the corresponding $F(\xi)$ are in Figs. 1b, 2b and 3b. $F(\xi)$ is always zero at the positions of the reactants and products, ξ_R and ξ_P, where the potential energy is a minimum, and at the transition state, ξ_{TS}, where $V(\xi)$ has a maximum. $F(\xi)$ has a minimum between the reactants and the transition state, at ξ_1, and a maximum between the transition state and the products, at ξ_2. These are the points of inflection of $V(\xi)$ and are indicated by vertical dotted lines in Figs. 1, 2 and 3. They define a rigorous partitioning of the process into three regions along the reaction

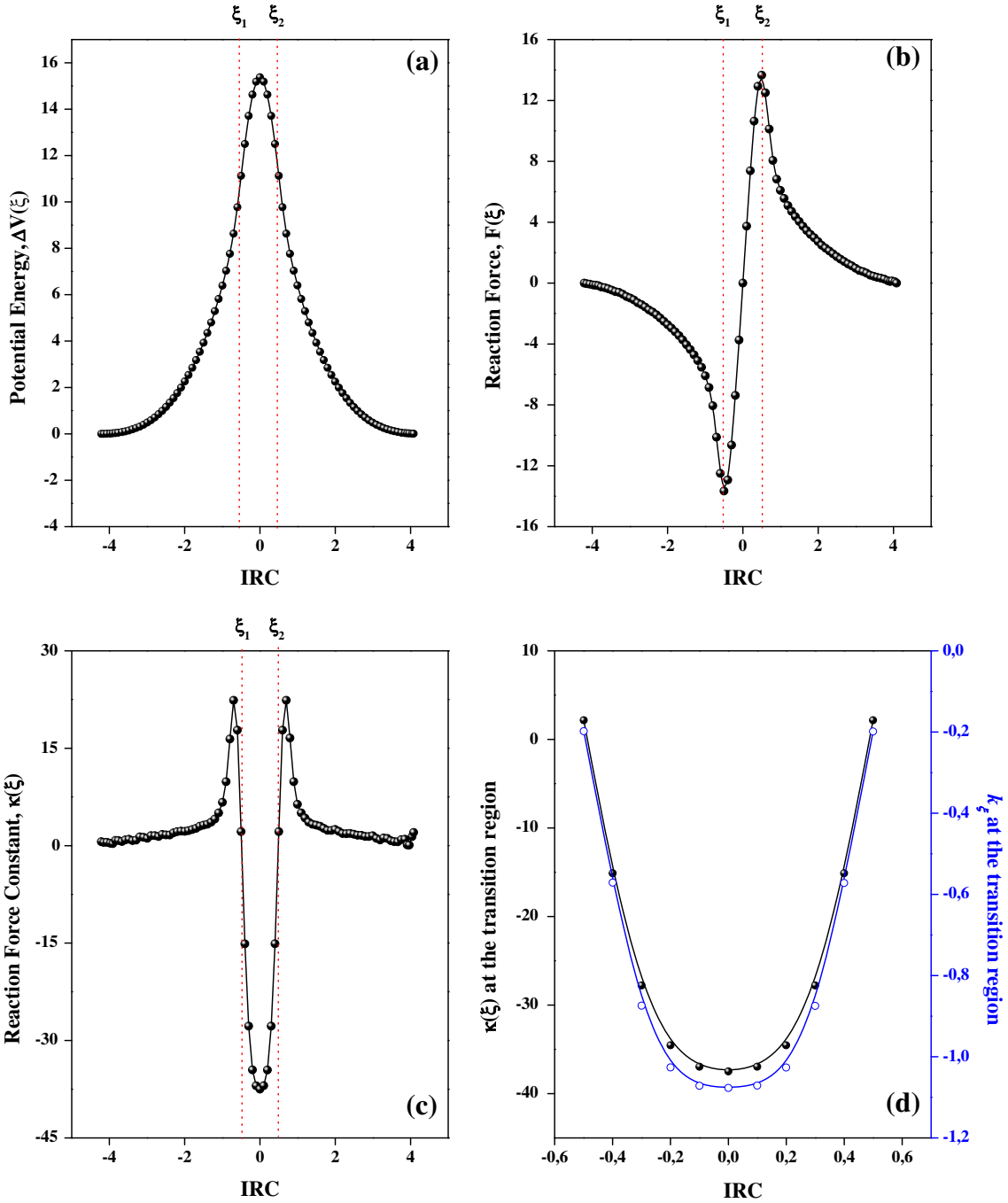

Fig. 1 Reaction **R1**: Profiles along IRC of a) $V(\xi)$, (b) $F(\xi)$, (c) $\kappa(\xi)$ and (d) $\kappa(\xi)$ and $k_\xi(\xi)$ in just the transition region between ξ_1 and ξ_2

coordinate: the reactant region, from **R** to the force minimum, the transition region, from the force minimum to the force maximum, and finally the product region, from the force maximum to **P**. Analyses of a variety of chemical reactions - proton transfers [3, 6], addition to a double bond [7, 8], bond dissociations [9–11], nucleophilic substitutions [12–14], nitro/aci tautomerization [15], and molecular rearrangements [16] - have revealed that each of the regions tends, in general, to emphasize a certain phase of the process, structural or electronic.

In the reactant region, $\xi_R \rightarrow \xi_1$, the focus is on structural changes in the reactants (bond stretching, angle bending, torsions, etc.), resulting in a distorted state of the reactants, at ξ_1, that is prepared for subsequent steps. Such structural changes are resisted by the reactants, so $F(\xi)$ is negative and therefore retarding, between ξ_R and ξ_1. In the second region, between ξ_1 and ξ_2, bond-breaking and bond-forming occur, normally accompanied by extensive electronic effects in properties such as the electrostatic potential, local ionization

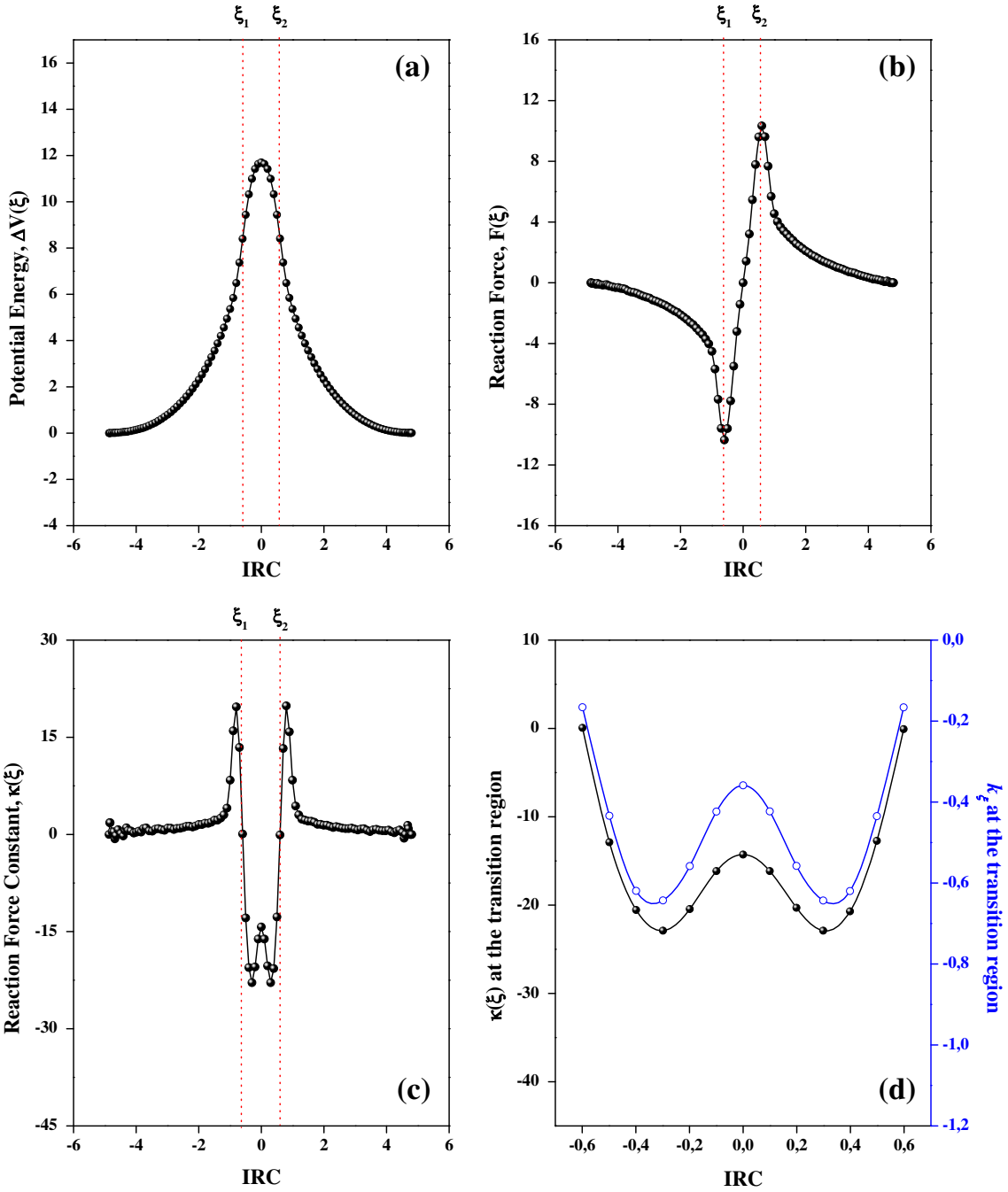

Fig. 2 Reaction **R2**: Profiles along IRC of (a) $V(\xi)$, (b) $F(\xi)$, (c) $\kappa(\xi)$ and (d) $\kappa(\xi)$ and $k_\xi(\xi)$ in just the transition region between ξ_1 and ξ_2

energy, reactivity descriptors, etc. After ξ_1, $F(\xi)$ includes an increasing positive driving component that gradually counteracts the retarding force. $F(\xi)$ reaches a maximum at ξ_2, where the system has arrived at a distorted state of the products, at ξ_2. In the final region, defined by the range $\xi_2 \rightarrow \xi_P$, structural relaxation takes place until the equilibrium geometries of the products are reached.

It is not being claimed that the different regions feature exclusively structural or electronic effects. Each region has both, but the structural are dominant in the first and third and the electronic in the second. In the first and third regions, the system can largely be viewed as manifesting the identities of the reactant(s) and product(s), respectively.

An important aspect of reaction force analysis is that the minimum of $F(\xi)$ provides a natural partitioning of the activation barrier ΔE_{act} into two components:

$$\Delta E_{act} = V(\xi_{TS}) - V(\xi_R) = [V(\xi_{TS}) - V(\xi_1)] + [V(\xi_1) - V(\xi_R)] = \Delta E_{act,2} + \Delta E_{act,1}. \quad (3)$$

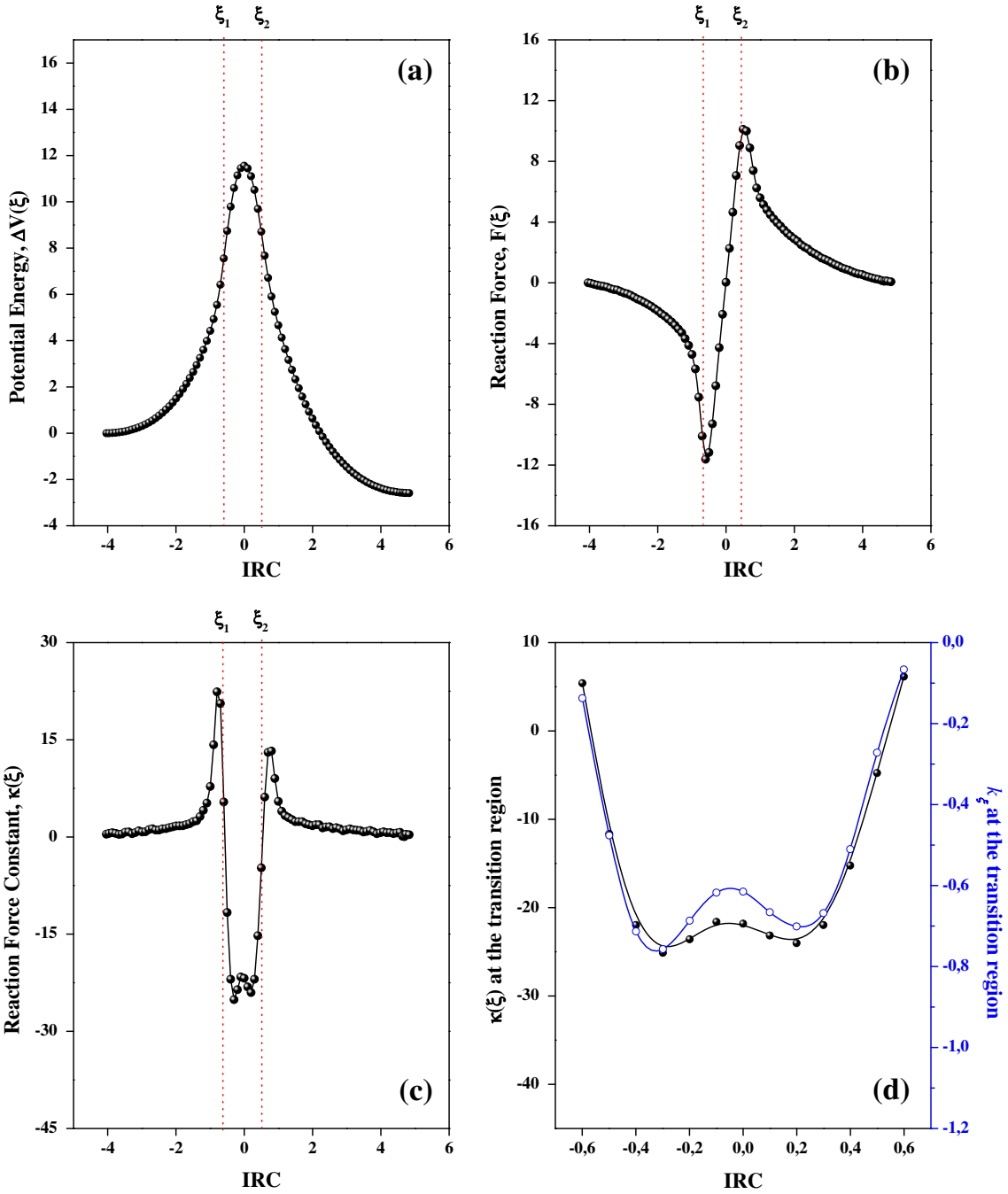

Fig. 3 Reaction **R3**: Profiles along IRC of (a) $V(\xi)$, (b) $F(\xi)$, (c) $\kappa(\xi)$ and (d) $\kappa(\xi)$ and $k_\xi(\xi)$ in just the transition region between ξ_1 and ξ_2

$\Delta E_{act,1}$ is the energy needed to overcome the resistance to the structural changes in the first region, while $\Delta E_{act,2}$ supports the electronic reorganization in the first stage of the transition to products, $\xi_1 \rightarrow \xi_{TS}$. The partitioning of ΔE_{act} into $\Delta E_{act,1}$ and $\Delta E_{act,2}$ helps to elucidate how an external agent, such as a catalyst or solvent, influences the rate of a process, *i.e.*, whether it affects primarily the structural or the electronic stages of the activation process. This has been demonstrated for both a catalyst [6] and a solvent [13], and will be seen again in this paper.

The net energy change in the entire transition region is given by

$$\Delta E_{transition} = V(\xi_2) - V(\xi_1) \tag{4}$$

The energy released in the final region, $\xi_2 \rightarrow \xi_P$, will be called $\Delta E_{relaxation}$, since it emphasizes structural relaxation from distorted products, at ξ_2, to their equilibrium states, at ξ_P.

$$\Delta E_{relaxation} = V(\xi_P) - V(\xi_2) \tag{5}$$

Taking into account all of the terms defined by Eqs. 3, 4 and 5, the overall energy of the process, ΔE°, is given by the sum of the contributions from the three regions:

$$\Delta E^{\circ} = \Delta E_{act,1} + \Delta E_{transition} + \Delta E_{relaxation}. \quad (6)$$

The reaction force constant

We have recently focused attention upon the reaction force constant $\kappa(\xi)$ along the reaction coordinate; this is the second-order derivative of $V(\xi)$[17–20]:

$$\kappa(\xi) = \frac{\partial^2 V(\xi)}{\partial \xi^2} = -\frac{\partial F(\xi)}{\partial \xi} \quad (7)$$

$\kappa(\xi)$ is a scalar quantity. Its behavior along ξ is displayed in Figs. 1c, 2c and 3c. $\kappa(\xi)$ is positive in the first and third regions and negative in the transition region, going through zero at the force minimum and maximum.

A significant feature of $\kappa(\xi)$ is that it has negative values throughout the *entire* transition region, not just at the maximum of $V(\xi)$. This focus upon the entire region rather than only a single point is totally in accord with Zewail and Polanyi's description of a continuum of transient, unstable states between unperturbed forms of the reactants and products [21, 22]. They arrived at this concept by a completely independent means, transition state spectroscopy. Their continuum of unstable states clearly corresponds to the transition region defined by the minimum and maximum of $F(\xi)$.

Present objectives

In earlier work [17, 23], the energetics and mechanism of the intramolecular proton transfer,

$$H - O - N = S \rightarrow O = N - S - H \quad (8)$$

were investigated. In the later study [17], the vibrational analysis was extended to nonstationary states along the IRC. The reactive mode, the movement of the proton from the oxygen to the sulfur, was observed to follow the IRC and its force constant along the IRC, $k_{\xi}(\xi)$, was computed. A striking similarity was found between $k_{\xi}(\xi)$ and the reaction force constant $\kappa(\xi)$, as obtained by Eq. 7. Both are positive in the first and third regions, pass through zero at the minimum and maximum of $F(\xi)$, and are negative throughout the entire transition region between ξ_1 and ξ_2.

In the present work, we have expanded this earlier analysis to include the three systems H-X-N = Y (X,Y = O,S), and to look at the effects of a water molecule in promoting the proton transfers. The presence of water was found to introduce a new pathway, the double proton transfer shown for each of the three systems in Scheme 1. Note that Scheme 1 displays not

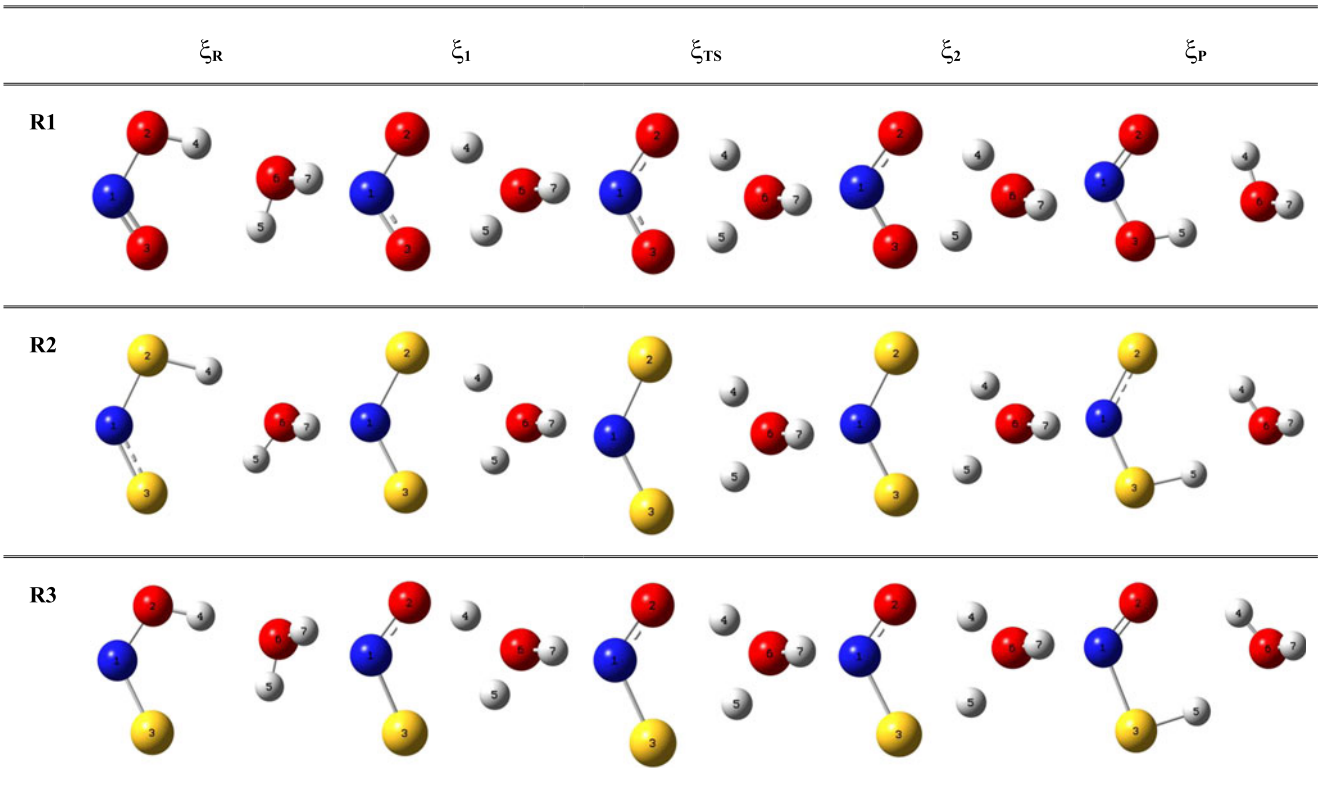

Scheme 1 The five key points along the water-assisted proton transfer reactions, HX-N=Y···H_2O → X=N-YH···H_2O (X,Y = O,S). Oxygens are in red, nitrogens in blue, sulfurs in yellow and hydrogens in white

only the reactants and products but also the systems at the $F(\xi)$ minimum, the $V(\xi)$ maximum and the $F(\xi)$ maximum.

Computational methods

Geometry optimizations of the stationary states along the IRC of each of the three reactions shown in Scheme 1 were performed with the hybrid exchange-correlation functional B3LYP [24–26] combined with the standard split-valence triple-ζ basis set augmented with d-type and p-type polarization functions, 6-311G(d,p). This computational protocol has been tested recently in other hydrogen transfer processes and predicted both reaction energies and activation barriers comparable to those obtained using high level post-Hartree-Fock methods [27]. The stationary states were confirmed through harmonic vibrational analyses, *i.e.*, zero- and one-imaginary frequency for energy minima and for transition states, respectively. As in our previous study [17], vibrational analyses were also performed for nonstationary states along each IRC, which was determined using a gradient reaction step size of 0.10 $amu^{1/2}$ bohr. All calculations were carried out with the Gaussian 03 suite of programs [28].

Results and discussion

Structural and vibrational analyses

We are looking at the water-assisted proton transfer reactions,

$$Y = N - X - H \cdots OH_2 \rightarrow X = N - Y - H \cdots OH_2 \quad (X, Y = O, S). \tag{9}$$

These proceed via an intermolecular double-proton-transfer mechanism (Scheme 1). The results will be compared to those obtained for the processes in the absence of water,

$$Y = N - X - H \rightarrow X = N - Y - H (X, Y = O, S) \tag{10}$$

studied earlier by Herrera et al. [23]. The reactions in Eq. 10 are intramolecular single proton transfers. Our objective is to gain insight into the mechanisms of the water-assisted processes, specifically the role of the water molecule. The force constant $k_\xi(\xi)$ corresponding to the reactive mode, the movement of the two protons, has been computed for each reaction, in order to assess the degree of similarity between $k_\xi(\xi)$ and $\kappa(\xi)$.

Table 1 Some computed bond lengths (Å) and bond angles (degs) at the five key points along the reaction pathways of the water-assisted double-proton-transfer reactions HX-N = Y···H_2O → X = N-YH···H_2O (X, Y = O,S). The values for this reaction in the absence of water are given in parentheses. All calculations were at the B3LYP/6-311G(d,p) level

Structure	ξ_R	ξ_1	ξ_{TS}	ξ_2	ξ_P
R1					
$d(O_2\text{-}H_4)$	1.000 (0.979)	1.146 (1.109)	1.361 (1.307)	1.505 (1.516)	2.274 (2.134)
$d(O_3\text{-}H_4)$	2.180 (2.133)	2.199 (1.516)	2.259 (1.307)	2.323 (1.108)	2.879 (0.979)
$A(O_2N_1O_3)$	114.7 (113.6)	115.8 (105.4)	115.8 (105.4)	115.8 (105.4)	114.8 (113.6)
$A(H_4O_2N_1)$	108.4 (105.8)	108.7 (85.1)	108.7 (77.3)	109.5 (71.1)	116.0 (62.6)
$d(O_6\text{-}H_4)$	1.749	1.304	1.116	1.017	0.967
$d(O_3\text{-}H_5)$	2.309	1.505	1.361	1.146	1.000
$d(N_1\text{-}O_6)$	3.294	2.822	2.816	2.822	3.279
R2					
$d(S_2\text{-}H_4)$	1.383 (1.374)	1.547 (1.501)	1.826 (1.744)	1.957 (2.009)	2.518 (2.883)
$d(S_3\text{-}H_4)$	2.914 (2.882)	2.826 (2.009)	2.850 (1.744)	2.888 (1.501)	3.250 (1.374)
$A(S_2N_1S_3)$	126.1 (125.2)	125.8 (111.8)	125.8 (111.7)	125.8 (111.8)	126.1 (125.2)
$A(H_4S_2N_1)$	103.1 (102.9)	98.0 (81.4)	96.5 (73.7)	96.6 (67.7)	100.6 (55.5)
$d(O_6\text{-}H_4)$	1.967	1.371	1.109	1.013	0.972
$d(S_3\text{-}H_5)$	2.520	1.957	1.826	1.547	1.383
$d(N_1\text{-}O_6)$	3.730	3.211	3.203	3.211	3.728
R3					
$d(O_2\text{-}H_4)$	1.008 (0.985)	1.150 (1.141)	1.414 (1.372)	1.530 (1.653)	2.199 (2.586)
$d(S_3\text{-}H_4)$	2.543 (2.426)	2.580 (1.848)	2.664 (1.664)	2.720 (1.463)	3.270 (1.353)
$A(O_2N_1S_3)$	119.4 (117.1)	119.3 (106.7)	119.3 (107.0)	119.1 (107.4)	117.1 (116.1)
$A(H_4O_2N_1)$	112.6 (108.5)	112.9 (92.3)	113.9 (86.1)	115.0 (80.4)	124.2 (70.6)
$d(O_6\text{-}H_4)$	1.684	1.303	1.082	1.009	0.966
$d(S_3\text{-}H_5)$	2.600	1.927	1.768	1.545	1.366
$d(N_1\text{-}O_6)$	3.373	2.989	2.992	3.005	3.578

Table 2 Vibrational frequencies (cm^{-1}) of $X_2N_1Y_3$ and $H_4X_2N_1$ bending and X_2H_4 stretching of HXNY (X,Y = O,S) molecules in the gas phase in the absence of a water molecule and in the presence of a water molecule

Vibrational mode	ν (gas phase)	ν (water complex)	Δν
R1			
$O_2N_1O_3$ bending	639	708	69
$H_4O_2N_1$ bending	1338	1461	123
O_2H_4 stretching	3588	3217	-371
R2			
$S_2N_1S_3$ bending	331	362	31
$H_4S_2N_1$ bending	1027	1084	57
S_2H_4 stretching	2458	2348	-110
R3 reactants			
$O_2N_1S_3$ bending	506	567	61
$H_4O_2N_1$ bending	1404	1527	123
O_2H_4 stretching	3451	3046	-405

In Figs. 1, 2 and 3 are the variations of $V(\xi)$, $F(\xi)$ and $\kappa(\xi)$ along the IRC, and $k_\xi(\xi)$ along the portion of it in the transition region, for the three water-assisted proton transfer reactions that are displayed in Scheme 1: **R1** (Fig. 1); **R2** (Fig. 2) and **R3** (Fig. 3). In Table 1 are reported some bond lengths and bond angles at the five key points along the IRC: reactants (ξ_R), $F(\xi)$ minimum (ξ_1), $V(\xi)$ maximum (ξ_{TS}), $F(\xi)$ maximum (ξ_2) and products (ξ_P). The values for the reactions in the absence of water are also given, in parentheses.

Table 1 shows that the presence of a water molecule markedly influences the structural effects in HXNY along the IRC. In the absence of water, there are significant changes in the $X_2N_1Y_3$ and $H_4X_2N_1$ bond angles, particularly the latter; they decrease quite considerably. These changes are necessary in order to bring the hydrogens close to the atoms to which they are being transferred. In the water-assisted processes, however, the transfers are through the waters and so these angles can remain, for the most part, nearly constant; the stretching of the bonds to the hydrogens being transferred are now the primary events.

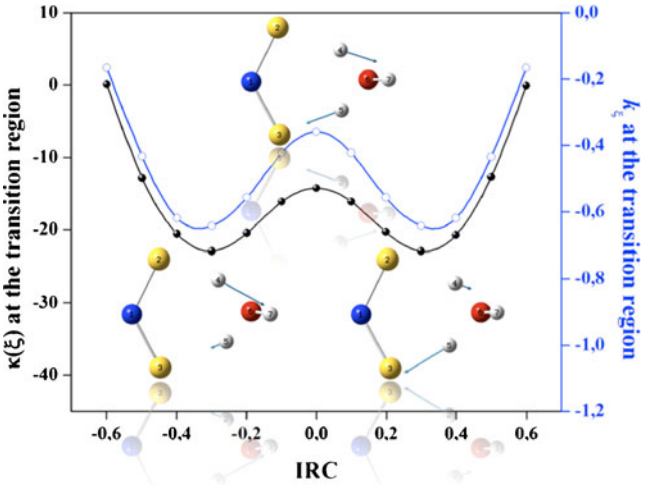

Fig. 4 Profiles of $\kappa(\xi)$ and $k_\xi(\xi)$ for **R2** in the transition region between ξ_1 and ξ_2, along with the structures of the reacting system at the two minima and the maximum of $\kappa(\xi)$. Blue lines indicate the directions and vibrational amplitudes of the migrating protons. The colors of the atoms are given in Scheme 1

These structural effects are consistent with the manner in which the water molecule influences the vibrational frequencies of the $X_2N_1Y_3$ and $H_4X_2N_1$ bending and X_2H_4 stretching modes. These frequencies are shown in Table 2, both with and without water being present. In all instances, both the $X_2N_1Y_3$ and the $H_4X_2N_1$ bending modes show a blue shift of their vibrational frequencies when a water molecule participates in the reaction. This suggests that the presence of the water imparts stiffness to these bending modes. In contrast, the X-H bond stretching undergoes a red shift in its vibrational frequency, indicating a weakening of this mode when a water molecule is involved. The first effect is most marked in the reactants and products of **R1** and **R3**.

Components of reaction energetics

In Figs. 1, 2 and 3 are displayed the potential energy and reaction force profiles for all of the water-assisted proton

Table 3 Reaction energetics computed at the B3LYP/6-311G (d,p) level for intramolecular proton transfer reactions without water, Eq. 10, and intermolecular water-assisted double-proton-transfer reactions, Eq. 9. ΔE_{int} is the interaction energy of the H-bonded complexes HXNY···H_2O (X,Y = O,S). All values are in kcal mol^{-1}

	$\Delta E_{act,1}$	$\Delta E_{act,2}$	ΔE_{act}	$\Delta E_{transition}$	$\Delta E_{relaxation}$	ΔE°	ΔE_{int}
Intramolecular-PT							
HONO	21.1	9.7	30.8	0.0	-21.1	0.0	
HSNS	15.7	7.6	23.2	0.0	-15.7	0.0	
HONS	17.8	8.7	26.5	-1.3	-23.4	-7.0	
Intermolecular-PT							
HONO···H_2O (R1)	11.1	4.2	15.4	0.0	-11.1	0.0	-11.1
HSNS···H_2O (R2)	8.4	3.3	11.7	0.0	-8.4	0.0	-7.5
HONS···H_2O (R3)	7.6	4.0	11.6	1.2	-11.3	-2.6	-11.2 (R) -6.8 (P)

transfer processes depicted in Scheme 1. The components of the reaction energetics defined in Eqs. 3, 4, 5, and 6 are given in Table 3 for both the intramolecular single proton processes, in the absence of water, Eq. 10, and the intermolecular water-assisted double-proton-transfer reactions, Eq. 9.

The presence of a water molecule has a striking effect upon all three activation energies, ΔE_{act}, reducing them by about 12 – 15 kcal mol^{-1}. A similar result was obtained in a computational study of water-assisted proton transfer in pterin [29].

The partitioning of the ΔE_{act} in Table 3 into their components $\Delta E_{act,1}$ and $\Delta E_{act,2}$ shows that the catalytic influence of the water is felt primarily in the first region; $\Delta E_{act,1}$ is lowered by roughly twice as much as $\Delta E_{act,2}$ in each case. As was pointed out already (in Structural and vibrational analyses), the presence of the water largely eliminates the need for the changes in the bond angles $X_2N_1Y_3$ and $H_4X_2N_1$ that are necessary in its absence; this lowers the energy requirements for the activation process in the water-assisted cases. The effect is particularly evident in $\Delta E_{act,1}$, since the changes in the $X_2N_1Y_3$ bond angle when water is not present are only in the first region, $\xi_R \rightarrow \xi_1$. Table 1 further shows that the water somewhat facilitates the stretching of the X_2H_4 bonds, through hydrogen bonding interactions. The water does also induce some electronic reorganization favoring *through-bond* interactions, as was shown in a previous study based on Kullback-Liebler information concepts [30].

Reaction force constant analysis

Figures 1, 2 and 3 show the reaction force constant $\kappa(\xi)$ along the IRC of each water-assisted proton transfer reaction in Scheme 1. $\kappa(\xi)$ is positive in the reactant and product regions, and negative throughout the entire transition region, which Zewail and Polanyi describe as a continuum of unstable, transient states [21, 22]. $\kappa(\xi)$ is zero at the force minimum and maximum and goes through maxima and minima at the inflection points of $F(\xi)$.

The $\kappa(\xi)$ profiles for these reactions show striking and intriguing differences in the transition regions. **R1** has a single minimum, at ξ_{TS}, corresponding to the inflection point in $F(\xi)$. **R2** has two symmetrical minima with a local maximum at ξ_{TS}, while **R3** has two asymmetrical minima. Very similar behavior is shown by the force constants $k_\xi(\xi)$ that correspond to the reactive modes of the processes, the movements of the protons from their initial to their final sites. The $k_\xi(\xi)$ are compared to the $\kappa(\xi)$ in each transition region in Figs. 1d, 2d and 3d. The asymmetry of the transition region minima in the case of **R3** is presumably due to one transfer being from oxygen to oxygen and the other from oxygen to sulfur.

To take a closer look at what is happening in the case where $\kappa(\xi)$ has two symmetrical minima, we show in Fig. 4 the $\kappa(\xi)$ and $k_\xi(\xi)$ profiles for **R2** in conjunction with the structures of the reacting system at the two minima and at the maximum. The blue lines indicate the directions and the vibrational amplitudes of the migrating protons. The active vibrational mode is dominated by the motion of the upper hydrogen at the first $\kappa(\xi)$ minimum and by that of the lower hydrogen at the second $\kappa(\xi)$ minimum. At the $\kappa(\xi)$ maximum, at ξ_{TS}, the vibrational motions of the hydrogens balance.

We want to emphasize that the fine structure observed in the transition regions of **R2** and **R3** for both $\kappa(\xi)$ and $k_\xi(\xi)$ is not readily evident in the respective $V(\xi)$ or even the $F(\xi)$ profiles. However it is revealed by $\kappa(\xi)$ - which is a rigorously-based physical property, the second derivative of $V(\xi)$. We believe that the fine structure reflects the degree of synchronicity of the two proton migrations in each case. The significance of this fine structure is being further investigated.

Conclusions

It has been shown that the presence of a water molecule promotes the proton transfer isomerization of HXNY (X,Y = O,S) by providing an intermolecular pathway whereby the hydrogen goes from X to the water, which in term sends another hydrogen to Y. This requires much smaller angular changes in the HXNY framework than does the intramolecular process when water is not present, and so the activation barriers are decreased significantly for the water-assisted cases.

A particularly interesting finding is the occurrence of local minima and maxima of $\kappa(\xi)$ within the transition regions of **R2** and **R3**. These features, the origins of which are being studied, demonstrate anew the importance of the entire region between the $F(\xi)$ minimum and maximum, not simply the point where $V(\xi)$ has its maximum.

Acknowledgments D. Y. is grateful to Comisión Nacional de Investigación Científica y Tecnológica, Gobierno de Chile (CONICYT) for a Ph.D. fellowship. The authors acknowledge the financial support by Fondo Nacional de Desarrollo Científico y Tecnológico, Chile (FONDECYT), grant number 1100291.

References

1. Toro-Labbé A (1999) J Phys Chem A 103:4398–4403
2. Jaque P, Toro-Labbé A (2000) J Phys Chem A 104:995–1003
3. Toro-Labbé A, Gutiérrez-Oliva S, Concha MC, Murray JS, Politzer P (2004) J Chem Phys 121:4570–4576
4. Fukui K (1981) Acc Chem Res 14:363–368
5. Gonzalez C, Schegel HB (1990) J Phys Chem 94:5523–5527

6. Rincón E, Jaque P, Toro-Labbé A (2006) J Phys Chem A 110:9478–9485
7. Burda JV, Murray JS, Toro-Labbé A, Gutiérrez-Oliva S, Politzer P (2009) J Phys Chem A 113:6500–6503
8. Jaque P, Toro-Labbé A, Geerlings P, De Proft F (2009) J Phys Chem A 113:332–344
9. Politzer P, Murray JS, Lane P, Toro-Labbé A (2007) Int J Quantum Chem 107:2153–2157
10. Politzer P, Murray JS (2008) Collect Czech Chem Commun 73:822–830
11. Murray JS, Toro-Labbé A, Clark T, Politzer P (2009) J Mol Model 15:701–706
12. Politzer P, Burda JV, Concha MC, Lane P, Murray JS (2006) J Phys Chem A 110:756–761
13. Burda JV, Toro-Labbé A, Gutiérrez-Oliva S, Murray JS, Politzer P (2007) J Phys Chem A 111:2455–2457
14. Echegaray E, Toro-Labbé A (2008) J Phys Chem A 112:11801–11807
15. Murray JS, Lane P, Göbel M, Klapötke TM, Politzer P (2009) Theor Chem Acc 124:355–363
16. Murray JS, Lane P, Nieder A, Klapötke TM, Politzer P (2010) Theor Chem Acc 127:345–354
17. Jaque P, Toro-Labbé A, Politzer P, Geerlings P (2008) Chem Phys Lett 456:135–140
18. Toro-Labbé A, Gutiérrez-Oliva S, Murray JS, Politzer P (2009) J Mol Model 15:707–710
19. Murray JS, Toro-Labbé A, Gutiérrez-Oliva S, Politzer P (2010) J Chem Phys 132:154308-154314
20. Politzer P, Reimers JR, Murray JS, Toro-Labbé A (2010) J Phys Chem Lett 1:2858–2862
21. Polanyi JC, Zewail AH (1995) Acc Chem Res 28:119–132
22. Zewail AH (2000) J Phys Chem A 104:5660–5694
23. Herrera B, Toro-Labbé A (2004) J Phys Chem A 108:1830–1836
24. Becke AD (1988) Phys Rev A 38:3098–3100
25. Lee CT, Yang WT, Parr RG (1988) Phys Rev B 37:785–789
26. Becke AD (1993) J Chem Phys 98:5648–5652
27. Gonzalez-Rivas N, Cedillo A (2005) J Chem Sci 117:555–560
28. Frisch MJ, Schlegel HB, Scuseria GE, Robb MA, Cheeseman JR, Montgomery JA Jr et al (2004) Gaussian 03, Revision E.01. Gaussian Inc, Wallingford
29. Jaramillo P, Coutinho K, Canuto S (2009) J Phys Chem A 113:12485–12495
30. Borgoo A, Jaque P, Toro-Labbé A, Van Alsenoy C, Geerlings P (2009) Phys Chem Chem Phys 11:476–482